SAND2019-15034R

Hydrogen diffusion across interfaces in zirconium

R.E. Jones*, R. Reyes†, X.-W. Zhou*,
M.E. Foster*, C.D. Spataru*, and D.E. Spearot†

*Sandia National Laboratories, Livermore, CA 94551
†University of Florida, Gainesville, FL 32611

Abstract

In order to study the effects of Ni oxidation barriers on H diffusion in Zr, a Ni-Zr-H potential was developed based on an existing Ni-Zr potential. Using this and existing binary potentials H diffusion characteristics were calculated and some limited findings for the performance of Ni on Zr coatings are made.

1 Introduction

The incorporation and transport of hydrogen in metals has wide technological interest. Zirconium, in particular, is well known to both absorb hydrogen and allow it to diffuse readily; however, the oxide that forms on the surfaces of zirconium is relatively impermeable. Nickel coatings prevent the formation of oxide layer on Zr and H transport in Ni is relatively fast. Zirconium has many phases/crystal structures depending on conditions and the Ni-Zr system can form alloys with a variety of compositions. At room temperature crystalline zirconium is hexagonally close-packed (HCP) α-Zr, and transitions to body-centered cubic β-Zr, at 1136 K. Nickel is face center cubic (FCC) at room temperature. As Fig. 1 in Tao *et al.* [1] shows these interfaces can be relatively sharp and form a stepped transition in composition from pure Zr to pure Ni.

This work focus on Ni-Zr interfaces using atomistic techniques to model the hydrogen diffusion. Generally speaking, embedded atom method (EAM) [2, 3] and modified embedded atom method (MEAM) [4] potentials are used to model these types of systems. Unfortunately, to our knowledge no Ni-Zr-H potential exists. For Ni-Zr alloys a number of parameterizations exist [5, 6, 7, 8, 9, 10] of various quality and tuned to different conditions. The EAM potential of Mendelev and coworkers

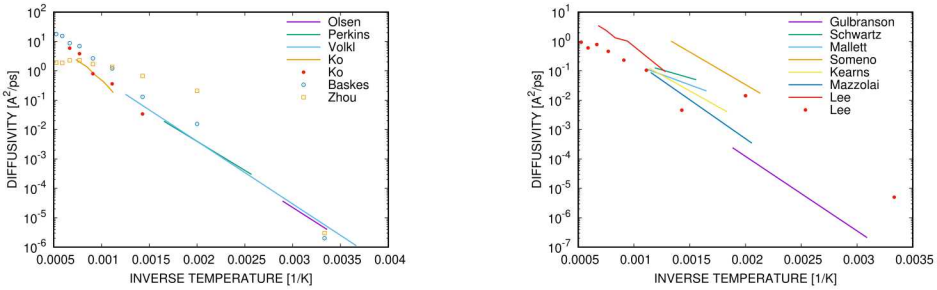

Figure 1: Comparison of diffusion versus inverse temperature for existing experimental and simulated data. Left panel: Ni-H, right panel: Zr-H. Lines: data obtained from literature, points: data obtained by us using published potentials.

[11, 8, 9] was parameterized to the liquid and glass properties of amorphous and crystalline NiZr alloys with application to solidification. An updated version is available through the NIST site (`https://www.ctcms.nist.gov/potentials/`) For the Ni-H system a number of parameterizations have been published [12, 13, 14, 15]. The work of Angelo *et al.* [12] is arguably the best. For the Zr-H system a number of parameterizations have also been published [16, 17, 18, 19, 18]. Only the MEAM potentials [15, 18] model hydrides with any fidelity. Other complexities than modeling bound hydrides with mobile diffusing H exist. Fig. 1 show the variety in predicted and measured Arrhenius behavior for both the Ni-H and Zr-H systems. For Ni-H the experiments are fairly consistent but there is scatter across predictions. For Zr-H the experiments and limited predictions both show inconsistencies.

In order to study and quantify hydrogen diffusion in Ni-Zr systems we needed to develop a Ni-Zr-H potential. Given our estimation of the quality of the existing potential and preliminary tests, two starting points seemed promising, one based on MEAM potentials and the other on an EAM potential. One would be to take the Lee and Lee Zr-H MEAM potential [18] and the Ko and Lee MEAM Ni-H potential [15] and add the Ni-Zr interactions. This would have the advantage of being able to model hydride formation; however, MEAM is more difficult to parameterize than EAM, the two potentials were not consistent in how they treated H, and the Ni-H showed instabilities for more than 1 H in the system. Instead we chose to add H interactions to the Mendelev Ni-Zr EAM potential [8].

2 Potential

The Embedded Atom Method (EAM) potential [2] in Finnis-Sinclair [20] form is

$$\Phi(r_{\alpha\beta}) = \underbrace{\sum_{a,\alpha\in\mathcal{G}_a} F_a\left(\sum_{b,\beta\in\mathcal{G}_b\neq\alpha} \rho_{ab}(r_{\alpha\beta})\right)}_{\text{embedded}} + \underbrace{\sum_{a,\alpha\in\mathcal{G}_a}\sum_{b,\beta\in\mathcal{G}_b\neq\alpha} \frac{1}{2}\phi_{ab}(r_{\alpha\beta})}_{\text{pair}} \tag{1}$$

where $F_a(\rho)$, $\rho_{ab}(r)$ and $\phi_{ab}(r)$ are functions. Suggested forms [21] for the embedding energy:

$$F_a(\rho) = f_a\left(\frac{\rho}{\varrho_a}\right)^{\eta_a}\left(\log\left(\left(\frac{\rho}{\varrho_a}\right)^{\eta_a}\right) - 1\right) \tag{2}$$

with minimum $-f_a$ at $\left(\frac{\rho}{\varrho_a}\right)^{\eta_a} = 1$ and three parameters $\{f_a, \eta_a, \varrho_a\}$, and the density:

$$\rho_{ab}(r) = \varrho_{ab}\exp(-\beta_{ab}r) \tag{3}$$

with two parameters $\{\rho_{ab}, \beta_{ab}\}$. The pair potential is taken to be in Morse form

$$\phi_{ab}(r) = E_{ab}\left(\exp(-2\alpha_{ab}(r - r_{ab})) - 2\exp(-\alpha_{ab}(r - r_{ab}))\right) \tag{4}$$

with three parameters $\{E_{ab}, \alpha_{ab}, r_{ab}\}$.

The Ni, Zr, and Ni-Zr parameters known from Ref. [8] which leaves eighteen unknown parameters: H self $\{f_H, \eta_H, \varrho_H\}$, $\{\varrho_{HH}, \beta_{HH}\}$, $\{E_{HH}, \alpha_{HH}, r_{HH}\}$; H with Ni $\{\varrho_{HNi}, \beta_{HNi}\}$, $\{E_{HNi}, \alpha_{HNi}, r_{HNi}\}$; and H with Zr: $\{\varrho_{HZr}, \beta_{HZr}\}$, $\{E_{HZr}, \alpha_{HZr}, r_{HZr}\}$ if we assume symmetry $\varrho_{ab} = \varrho_{ba}$ and $\beta_{ab} = \beta_{ba}$. The properties of pure Ni and Zr predicted by the Mendelev EAM potential are given in Table 1 and Table 2. It is noteworthy that the Mendelev EAM potential predicted negative interface energies for Ni:Zr interfaces which suggests a propensity for mixing as opposed to sharp interfaces.

Given the number of unknown parameters we decided to calibrate two potentials, (a) a simplified Ni-Zr-H potential where the EAM M:H interactions have been reduced to the Morse pair potential (NiZr+H in the remainder of this report), *i.e.* $F_H(\rho) = 0$ and $\rho_{MH}(r) = 0$, and (b) the full Ni-Zr-H EAM potential (NiZrH in the remainder). Here, $M \in \{$ Ni, Zr $\}$.

We calculated training data using density functional theory (DFT) simulations (with VASP (`https://www.vasp.at`) specific to the diffusion process. With a 54 atom cell for both a HCP Zr lattice and a FCC Ni lattice, we used the nudged elastic band (NEB) method to have a single H traverse between neighboring tetrahedral

	exp.	DFT	MD
a(Å)	3.52	3.52	3.52
E_c(eV/atom)		-5.07	-4.39
C11(GPa)	252	272	247
C12(GPa)	152	159	147
C44(GPa)	123	130	122

Table 1: Ni (FCC). Experimental values from Refs. [22, 23, 24].

	exp.	DFT	MD
a(Å)	3.23	3.23	3.22
c(Å)	5.15	5.17	5.28
E_c(eV/atom)	-6.32	-6.39	-6.47
C11(GPa)	155	136	156
C33(GPa)	172	160	180
C12(GPa)	67	72	77
C13(GPa)	65	66	63
C44(GPa)	36	32	48
C55(GPa)		24	33

Table 2: Zr (HCP). Experimental values from Refs. [25, 19].

(TET) and octahedral (OCT) interstitial sites and recorded changes in system volume and energy. This data is relevant to the diffusion process since it characterizes the energy barrier and configurational changes for the most likely diffusion path, it also quantifies the relative stability of H in the TET and OCT sites. The DFT data in Fig. 2 (black) shows that the OCT site is relatively stable in Ni whereas the TET site is more stable in Zr. Also H prefers neighboring locations to the TET site. In both systems the insertion of H causes swelling. Fig. 3 shows that insertion energy for 2 H in Ni or Zr has now clear dependence on H-H distance, which is a problem for the usual paradigm for empirical interatomic potentials and may be a small system effect. Also the energy-volume behavior shows a clearer trend but no ordering with respect to the site locations.

In calibrating both the simplified NiZr+H and full NiZrH potentials we wish to capture stability of H in interstitial sites, the diffusion energy barriers, swelling volumes, and H-H coordination effects in metal lattice. For the diffusion path data we employed corresponding NEB calculation in our molecular dynamics code (LAMMPS `https://lammps.sandia.gov`). For the H-H coordination effects we employed calculations similar to the DFT simulations. We used same 54 atom Ni and Zr lattices as in the DFT calculations but replicated 2×2×2 to avoid self-interaction issues. Use weighted least squares error based on relative error in the relevant data, *e.g.* changes in volume and energy for the super-cell. We fit the calculated properties with a genetic algorithm [26]. Fig. 4 shows an example of the data produced by the genetic optimization in the case where the optimization converged.

Given that the simplified NiZr+H potential only has M-H pair interactions, the M-H and H-H data can be fit sequentially. In fitting the diffusion data in Fig. 2 we found that the pair potential always caused cell shrinkage when it came close to fitting the energy data. Given this model discrepancy, we decided only to fit the energy data. Also given that the H-H data not consistent with a distance based potential we assume a small repulsive energy to ensure multiple H do not occupy the same site. The resulting parameters are given in Table 3.

Although the full NiZrH potential should be able to represent the volume swelling as well as the energy barrier of the NEB calculations, fitting it was less successful. We believe this was due to the much larger number of parameters and some correlations between the parameters. Augmenting the DFT training data with systems with Ni, Zr and H constituents did appear to help but a satisfactory potential was not obtained during the project.

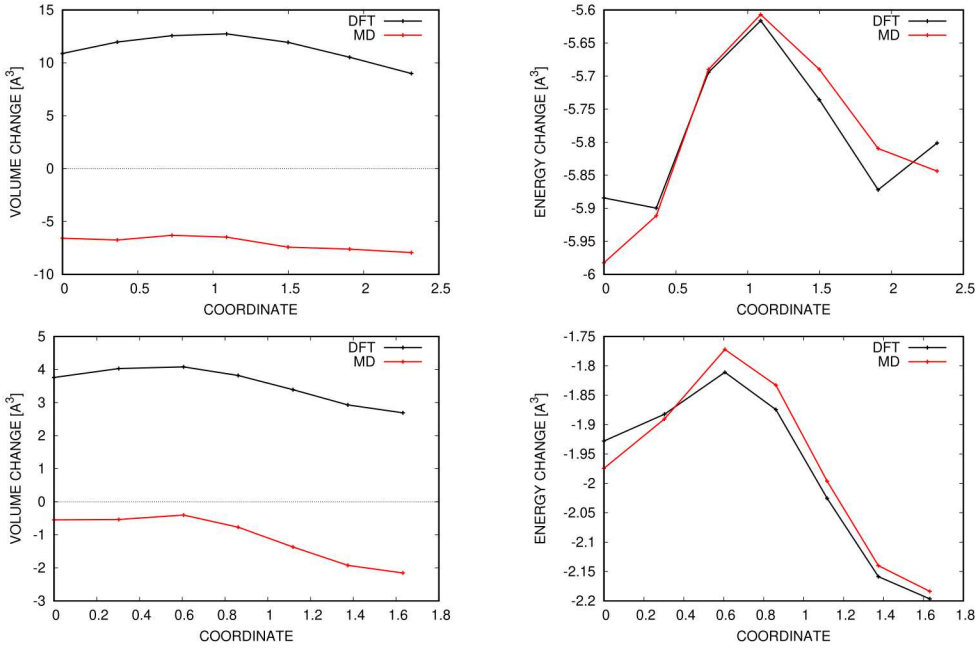

Figure 2: H in metal lattice volume change and energy change as a function of the TET to OCT path reaction coordinate. Upper panels: Zr-H (barrier 0.28 eV), lower panels: Ni-H (barrier 0.12 eV).

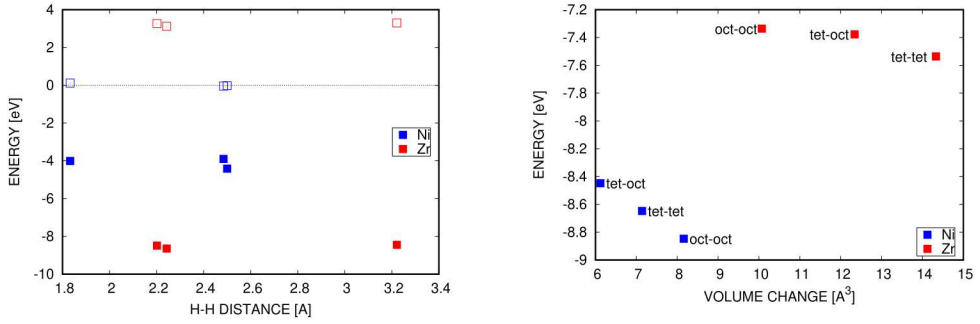

Figure 3: H-H in metal coordination effects. Left panel energy as a function of H-H distance (for open symbols the H self energy has been subtracted), right panel energy *vs.* system volume change.

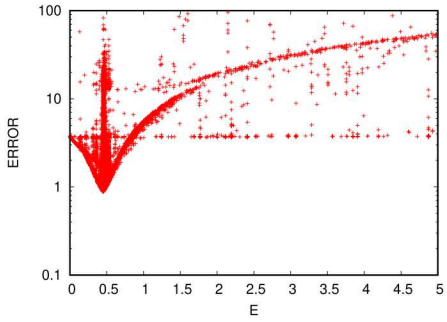

Figure 4: Genetic algorithm fit error for simplified NiZr+H potential projected onto the E_{NiH} parameter.

	NiH	ZrH
E	0.441054	1.459919
a	2.828092	1.870996
r	1.512915	1.675497

Table 3: NiZr+H EAM+Morse potential parameters.

3 Diffusion

Diffusion of atomic hydrogen in a solid lattice is a well studied phenomenon, see Ref. [27, Chap.4] for example. As mentioned, the small H atoms prefer to reside in interstitial sites and hop/diffuse between them. The Green-Kubo relation

$$\mathbf{D} = \frac{1}{3}\int_0^\infty \langle \bar{\mathbf{v}}_a(0) \otimes \bar{\mathbf{v}}_a(t)\rangle \,\mathrm{d}t \approx \frac{1}{N_a}\sum_{\alpha\in\mathcal{G}_a}\int_0^\infty \langle \mathbf{v}_\alpha(0)\otimes\mathbf{v}_\alpha(t)\rangle\,\mathrm{d}t \tag{5}$$

provides an equilibrium, small cell molecular dynamics (MD) method for estimating the diffusivity matrix $\mathbf{D}$ and the mean diffusion constant $D = \operatorname{tr}\mathbf{D}$. Here $\bar{\mathbf{v}}_a$ is the species a average velocity, $\mathbf{v}_\alpha$ is the velocity of atom α, and $\mathcal{G}_a$ group of all atoms of species a. For dilute systems the GK expression reduces to the usual Einstein relation. Despite H being relatively mobile in the Ni and Zr, we needed to employ temperature acceleration to get reliable estimates on MD timescales. If we assume Arrhenius behavior

$$D(T) = D_0 \exp\left(-\frac{E}{k_B T}\right) \tag{6}$$

with a single barrier with height E, temperature T, and Boltzmann constant k_B, we can use this relation to calculate D at higher temperatures and then estimate D at

room temperature.

After conducting preliminary simulations to estimate system size effects and concentration effects, we ran equilibrium simulations from 300 K to 2000 K for H in Ni and in Zr lattices. It was crucial to find the range where the H were mobile and the lattice was still solid and crystalline, so we monitored the M-H and M-M radial distribution functions (RDFs) to find the range over which the Arrhenius relation can be fit.

Fig. 5 shows the mean-squared displacement of the H diffusion/random walk for a sequence of temperatures. Clearly the expected $\langle x^2 \rangle \sim t$ relation holds for a sufficiently high temperature. This behavior is corroborated by the H-Zr RDF which shows that the zero occupation valleys disappear as the temperature increases. Correspondingly where Zr-Zr RDF shows a lack of distinct peaks separated by zero occupation valleys indicates where the Zr has lost crystallinity. These two temperature bounds define the appropriate range to fit the $D(1/T)$ data and hence determine an estimate for D at T= 300 K.

Using this method and the simplified NiZr+H potential we were able compare the results of this ternary potential to those for existing binary potentials for Zr-H and Ni-H. Fig. 6 indicates that the new ternary potential gives diffusion estimates comparable to the more trusted existing binary potentials. Note for Zr-H we also calculated H diffusion constant for the c-axis separately from the a-plane. Since these estimates were similar to within uncertainty and are not shown for clarity.

Lastly, we attempted to obtain the diffusion properties for H near a Ni:Zr interface using a novel analysis. Unfortunately, the Ni:Zr bi-crystal systems were not stable at elevated temperatures with the Mendelev EAM potential we built our NiZr+H potential upon. It appears that the interface energy predicted by the potential it too negative and hence mixing/alloying is preferred to interface stability. In lieu of stable interfaces we calculated the H diffusion constants in a range of amorphous Ni-Zr alloys. Although not entirely converged with respect to amorphous configuration samples, the results show that if intervening amorphous layers exist between Ni and Zr and they are high in Zr content, they could be prohibitive barriers to H diffusion.

4 Discussion

The findings of this project were:

- a potential more complex than a pair-wise potential is probably needed to represent both the H diffusion energy barrier and the H swelling volume in Ni and Zr,

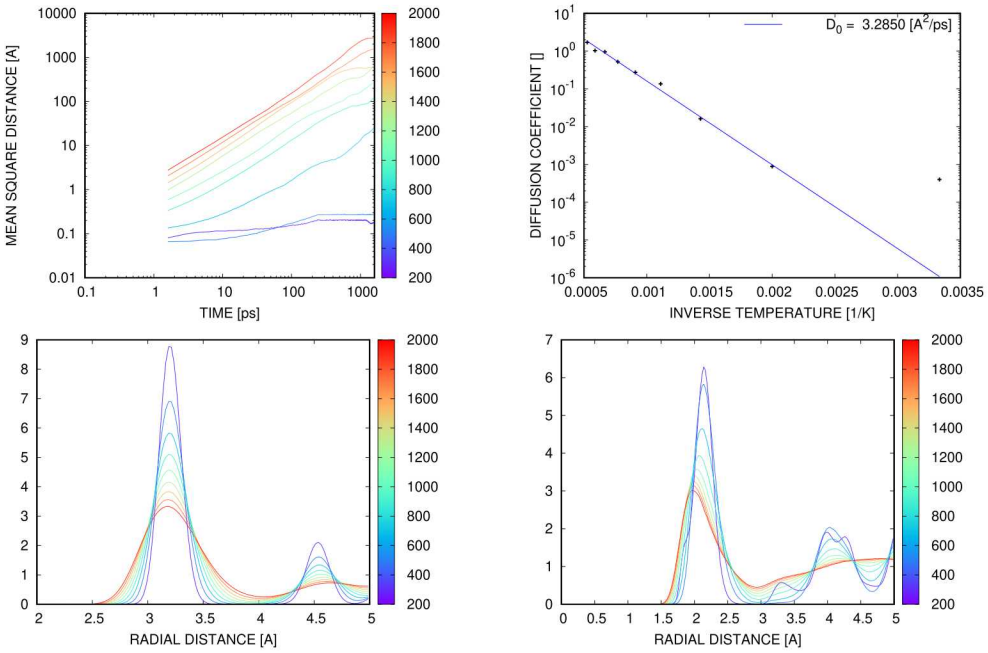

Figure 5: H diffusion in Zr. Upper left panel: mean squared displacement as a function of time for a sequence of temperatures. Upper right panel: Arrhenius plot of the diffusion coefficient as a function of inverse temperature. Lower left panel: Zr-Zr radial distributions for a sequence of temperatures. Lower right panel: Zr-H radial distributions for a sequence of temperatures.

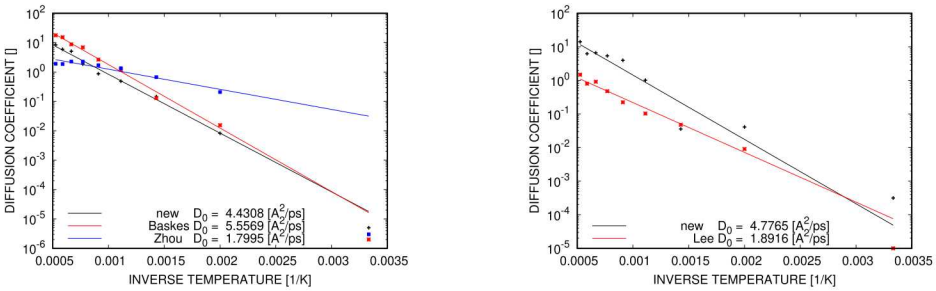

Figure 6: Comparison of the Arrhenius behavior of the NiZr+H potential with existing binary potentials. Left: Ni-H, right: Zr-H.

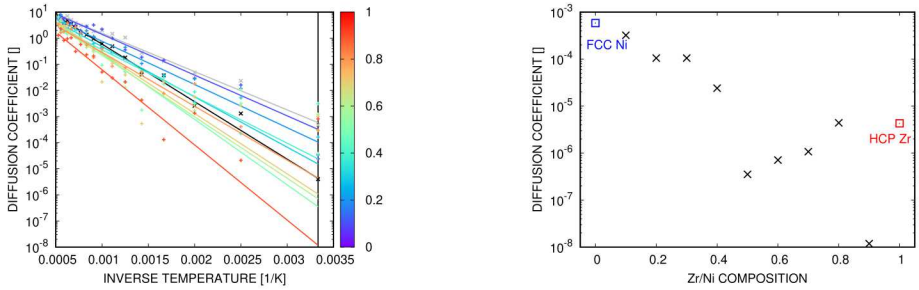

Figure 7: H diffusion in amorphous Ni-Zr alloys. Left: Arrhenius behavior for the alloys (colored by Zr fraction), right: diffusion constant as a function of Zr fraction with crystalline Ni and Zr results shown for comparison.

- a NiZr+H potential that captured the H diffusion barrier was parameterized and produced diffusion behavior comparable to existing binary potentials,
- the potential predicted that NiZr has a strong propensity to mix species and destabilize interfaces at elevated temperatures,
- in amorphous, Zr rich, NiZr alloys the H diffusion can be severely limited which has some relevance to coating Zr with Ni to maintain good H diffusion.

In addition to focusing on the NiZrH system we were also able to perform preliminary studies of H diffusion in ZrO_2 and ZrO_2:Zr interfaces. Unfortunately the available COMB potential [28] is computationally expensive and also does not seem to model H diffusion well. Other potentials exist for the ZrO system [29, 30, 31, 32] but were not evaluated due to a lack of H interactions. Given the importance of hydride formation and the proclivity of the Mendelev potential to mix, work is underway to refit entire potential under other funding. Lastly, the DFT training data for NiH and ZrH including additional data for amorphous Ni-Zr-H and crystalline Zr-O-h is available upon request (`rjones@sandia.gov`).

Acknowledgments

This work was supported by the Tritium Science Program (David Senor, Pacific Northwest National Laboratory, Project Manager). This funding is gratefully acknowledged. Sandia National Laboratories is a multimission laboratory managed and operated by National Technology and Engineering Solutions of Sandia, LLC., a wholly owned subsidiary of Honeywell International, Inc., for the U.S. Department of

Energy's National Nuclear Security Administration under contract DE-NA0003525. The views expressed in the article do not necessarily represent the views of the U.S. Department of Energy or the United States Government.

References

[1] Xiaoma Tao, Pei Yao, Wenwang Wei, Hongmei Chen, Yifang Ouyang, Yong Du, Yuan Yuan, and Qing Peng. An experimental study on the interdiffusion behaviors and mechanical properties of ni-zr system. *Journal of Alloys and Compounds*, 752:412–419, 2018.

[2] Murray S Daw, Stephen M Foiles, and Michael I Baskes. The embedded-atom method: a review of theory and applications. *Materials Science Reports*, 9(7-8):251–310, 1993.

[3] Murray S Daw and Michael I Baskes. Embedded-atom method: Derivation and application to impurities, surfaces, and other defects in metals. *Physical Review B*, 29(12):6443, 1984.

[4] Michael I Baskes. Modified embedded-atom potentials for cubic materials and impurities. *Physical review B*, 46(5):2727, 1992.

[5] Carlo Massobrio, V Pontikis, and G Martin. Amorphization induced by chemical disorder in crystalline $NiZr_2$: a molecular-dynamics study based on an n-body potential. *Physical review letters*, 62(10):1142, 1989.

[6] R Devanathan, NQ Lam, PR Okamoto, and M Meshii. Molecular-dynamics simulation of electron-irradiation-induced amorphization of $NiZr_2$. *Physical Review B*, 48(1):42, 1993.

[7] B Böddeker and H Teichler. Dynamics near free surfaces of molecular dynamics simulated ni 0.5 zr 0.5 metallic glass films. *Physical Review E*, 59(2):1948, 1999.

[8] MI Mendelev, MJ Kramer, SG Hao, KM Ho, and CZ Wang. Development of interatomic potentials appropriate for simulation of liquid and glass properties of $NiZr_2$ alloy. *Philosophical Magazine*, 92(35):4454–4469, 2012.

[9] SR Wilson and MI Mendelev. Anisotropy of the solid–liquid interface properties of the Ni–Zr B33 phase from molecular dynamics simulation. *Philosophical Magazine*, 95(2):224–241, 2015.

[10] MH Yang, SN Li, Y Li, JH Li, and BX Liu. Atomistic modeling to optimize composition and characterize structure of Ni–Zr–Mo metallic glasses. *Physical Chemistry Chemical Physics*, 17(20):13355–13365, 2015.

[11] Mikhail I Mendelev and Graeme J Ackland. Development of an interatomic potential for the simulation of phase transformations in zirconium. *Philosophical Magazine Letters*, 87(5):349–359, 2007.

[12] James E Angelo, Neville R Moody, and Michael I Baskes. Trapping of hydrogen to lattice defects in nickel. *Modelling and Simulation in Materials Science and Engineering*, 3(3):289, 1995.

[13] Barbara Szpunar, Laurent J Lewis, Ian Swainson, and Uwe Erb. Thermal expansion and hydrogen diffusion in nanocrystalline nickel. *Physical Review B*, 60(14):10107, 1999.

[14] XW Zhou, RA Johnson, and HNG Wadley. Misfit-energy-increasing dislocations in vapor-deposited CoFe/NiFe multilayers. *Physical Review B*, 69(14):144113, 2004.

[15] Won-Seok Ko, Jae-Hyeok Shim, and Byeong-Joo Lee. Atomistic modeling of the Al–H and Ni–H systems. *Journal of Materials Research*, 26(12):1552–1560, 2011.

[16] Kenji Konashi, Tamio Ikeshoji, Yoshiyuki Kawazoe, and Hideki Matsui. A molecular dynamics study of thermal conductivity of zirconium hydride. *Journal of Alloys and compounds*, 356:279–282, 2003.

[17] Eduard Pastukhov, Nikolay Sidorov, Andrey Vostrjakov, and Victor Chentsov. Molecular dynamic simulation of short order and hydrogen diffusion in the disordered metal systems. In *Molecular Dynamics-Theoretical Developments and Applications in Nanotechnology and Energy*. InTech, 2012.

[18] Byeong-Moon Lee and Byeong-Joo Lee. A comparative study on hydrogen diffusion in amorphous and crystalline metals using a molecular dynamics simulation. *Metallurgical and Materials Transactions A*, 45(6):2906–2915, 2014.

[19] Ravi Kiran Siripurapu, Barbara Szpunar, and Jerzy A Szpunar. Molecular dynamics study of hydrogen in α-zirconium. *International Journal of Nuclear Energy*, 2014, 2014.

[20] MW Finnis and JE Sinclair. A simple empirical n-body potential for transition metals. *Philosophical Magazine A*, 50(1):45–55, 1984.

[21] Xiaowang W Zhou, R Dingreville, and Richard A Karnesky. Molecular dynamics studies of irradiation effects on hydrogen isotope diffusion through nickel crystals and grain boundaries. *Physical Chemistry Chemical Physics*, 20(1):520–534, 2018.

[22] JR Neighbours, FW Bratten, and Charles S Smith. The elastic constants of nickel. *Journal of Applied Physics*, 23(4):389–393, 1952.

[23] Hassel M Ledbetter and Richard Palmer Reed. Elastic properties of metals and alloys, I. iron, nickel, and iron-nickel alloys. *Journal of Physical and Chemical Reference Data*, 2(3):531–618, 1973.

[24] Hakaru Masumoto, Hideo Saitô, Yûetsu Murakami, and Michio Kikuchi. Crystal anisotropy and temperature dependence of young's modulus in single crystal of nickel. *Transactions of the Japan Institute of Metals*, 10(2):119–123, 1969.

[25] Zizhe Lu, Aleksandr Chernatynskiy, Mark J Noordhoek, Susan B Sinnott, and Simon R Phillpot. Nanoindentation of zr by molecular dynamics simulation. *Journal of Nuclear Materials*, 467:742–757, 2015.

[26] John Eddy and Kemper Lewis. Effective generation of pareto sets using genetic programming. In *Proceedings of ASME Design Engineering Technical Conference*, volume 132, 2001.

[27] Daan Frenkel and Berend Smit. *Understanding molecular simulation: from algorithms to applications*, volume 1. Elsevier, 2001.

[28] Zizhe Lu, Aleksandr Chernatynskiy, Mark J Noordhoek, Susan B Sinnott, and Simon R Phillpot. Nanoindentation of ZrO_2 and ZrO_2/Zr systems by molecular dynamics simulation. *Journal of Nuclear Materials*, 486:250–266, 2017.

[29] M áSakib Khan, M áSaiful Islam, and DavidáR Bates. Cation doping and oxygen diffusion in zirconia: a combined atomistic simulation and molecular dynamics study. *Journal of Materials chemistry*, 8(10):2299–2307, 1998.

[30] KV Damodaran, VS Nagarajan, and KJ Rao. A molecular dynamics study of ZrO_2 SiO_2 system. *Journal of non-crystalline solids*, 124(2-3):233–241, 1990.

[31] Martin Kilo, Christos Argirusis, Günter Borchardt, and Robert A Jackson. Oxygen diffusion in yttria stabilised zirconia-experimental results and molecular dynamics calculations. *Physical Chemistry Chemical Physics*, 5(11):2219–2224, 2003.

[32] S Arash Sheikholeslam, Weijun Luo, Cristian Grecu, Guangrui Maggie Xia, and André Ivanov. Hydrogen diffusion in amorphous zro2. *Journal of Non-Crystalline Solids*, 440:7–11, 2016.